SCANNING PROBE MICROSCOPY – PHYSICAL PROPERTY CHARACTERIZATION AT NANOSCALE

Edited by **Vijay Nalladega**

INTECHOPEN.COM

Scanning Probe Microscopy – Physical Property Characterization at Nanoscale
Edited by Vijay Nalladega

Published by InTech
Janeza Trdine 9, 51000 Rijeka, Croatia

Publishing Process Manager Oliver Kurelic
Technical Editor Teodora Smiljanic
Cover Designer InTech Design Team

First published April, 2012
Printed in Croatia

A free online edition of this book is available at www.intechopen.com
Additional hard copies can be obtained from orders@intechopen.com

Scanning Probe Microscopy – Physical Property Characterization at Nanoscale,
Edited by Vijay Nalladega
p. cm.
ISBN 978-953-51-0576-3

Contents

5

Characterization of Complex Spintronic and Superconducting Structures by Atomic Force Microscopy Techniques

L. Ciontea[1], M.S. Gabor[1], T. Petrisor Jr.[1],
T. Ristoiu[1], C. Tiusan[1,2] and T. Petrisor[1]
[1]*Technical University Cluj-Napoca, Material Science Laboratory, Napoca*
[2]*Institut Jean-Lamour, UMR7198 CNRS-Nancy Université, Vandoeuvre les Nancy*
[1]*Romania*
[2]*France*

1. Introduction

Within this chapter we would like to address two main applications of Atomic Force Microscopy techniques. The first one illustrates the use of the Atomic Force Microscopy for the optimization of the morphological properties in multilayer stacks dedicated to spintronic devices, in which the electric current flows perpendicular to the layers (current-perpendicular-to-plane CPP geometry). The second part of our chapter presents the use of the Magnetic Force Microscopy as a tool for the micro-magnetic characterization of magnetic thin film dedicated to interface systems with high temperature superconductors. The performances of both spintronic and superconductor/ferromagnet interface devices are directly related to the optimal structural and magnetic properties of the constituent thin films. During the process of the complex sample growth, the structural, morphological and magnetic characterization represents one of the most important steps. Various ex-situ techniques are involved for characterization at microscopic and macroscopic scale. For the multilayer stacks, which require flatness and continuity of the constituent layers, the near field microscopy techniques represent one of the most commonly used tools. The standard atomic force microscopy (AFM) allows to extract precise information about the thin film surface topology in terms of roughness and morphology. This information is furthermore correlated with the crystallographic properties of the layers determined by diffraction techniques (X-Ray, electrons…). The magnetic force microscopy (MFM) operating mode provides a complete characterization of the micromagnetic properties of a magnetic film. This analysis at a microscopic scale is often correlated to the macroscopic magnetic properties measured using the magnetometry techniques.

2. The use of AFM technique for the characterization of multilayer stacks for spintronic devices

After the discovery in 1989 of the giant magnetorezistive effect in magnetic multilayers by A. Fert and P. Grunberg (Baibich et al 1988, Binash et al 1989), the spintronics became one of

the most attractive research fields from both fundamental and applicative point of view. The spintronic devices, composed by alternating magnetic and nonmagnetic multilayer structures, represent nowadays one of the major issues of the sensors and data storage industries (Wolf et al 2001). The main functional property of a spintronic device is based on the skilful manipulation of the spin of the electrons carrying the charge current.

In the current-perpendicular-to-plane (CPP) spintronic devices, the interfacial roughness has to be minimized in order to get flat and abrupt interfaces between the different layers. This avoids the intermixing and provides a perfect continuity with minimum thickness fluctuations of spacers sandwiched between adjacent layers. We chose to show here the characterization steps by AFM in a complex magnetic tunnel junction multilayer stack using as magnetic electrodes the full Heusler Co_2FeAl film and the single crystal MgO as insulating barrier. Therefore, the magnetic tunnel junction is constituted of the MgO insulating barrier sandwiched between two magnetic metallic films (Tiusan et al 2007) (transition metal and Heusler alloy). The electric current crosses the insulator by quantum tunneling whose thickness is typically less than 12 monolayers. Therefore, one can easily understand that the extreme control of the interfacial roughness is a key parameter for proper operating the device. Analysis of our samples by AFM provides the surface topography of the layers. This has been correlated with their crystalline structure analyzed by X ray diffraction techniques. Our analysis allowed a deep understanding of the growth mechanisms by the sputtering of the layers constituent of the complex multilayer stack.

The Co_2FeAl (CFA) Heusler alloy has a cubic structure with a lattice parameter close to 0.573 nm. For this reason, in order to facilitate the epitaxial growth of the Heusler alloy, one can use single crystalline MgO(001) substrates. The MgO has a crystalline structure belonging to the Fm-3m space group, essentially formed by the interpenetration of two face centered cubic sub-lattices containing Mg and O atoms. Taking into account the CFA and MgO lattice parameters, the CFA should normally grow on MgO with the epitaxial relation: CFA(001)[110]||MgO(001)[100], which implies a 45° in-plane rotation of the CFA lattice with respect to the MgO one. In this configuration the lattice mismatch between CFA and MgO is $(\sqrt{2}/2a_{CFA} - a_{MgO})/a_{MgO} = -3.8\%$, which is adequate to promote epitaxy. However, in order to better adapt the lattice mismatch between the epitaxial film and the single crystalline substrate one can employ a buffer layer. We explored this possibility by using an epitaxial Cr film as buffer. Cr has a body centered cubic crystalline structure belonging to the Im-3m space group. The lattice parameter is 0.2884 nm and if one assumes a Cr(001)[110]||MgO(001)[100] epitaxial relation of Cr on MgO, the lattice mismatch is -3.15%. Moreover, considering a cube-on-cube epitaxy of CFA on Cr, i.e. CFA(001)[100]||Cr(001)[100] (see figure 1), the lattice mismatch between CFA and Cr is only -0.7%, and as a consequence, Cr is well suited to be used as a buffer layer for the epitaxial growth of CFA films on MgO(001) substrates.

2.1 Chromium buffer layer

Although CFA Heusler alloy thin films were also grown on un-buffered MgO (001) single crystal substrates, we will first discuss the epitaxial growth of Cr (001) buffer layer. The process of epitaxial growth of CFA on MgO is essentially similar to that of Cr on MgO, even

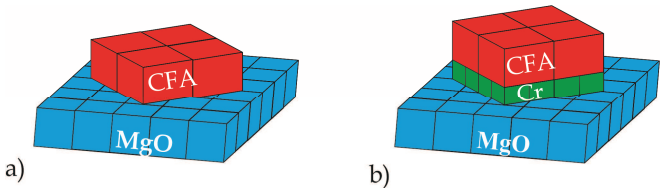

Fig. 1. Schematic representation of the (a) CFA and (b) Cr/CFA bilayer epitaxy on MgO(001) single crystalline substrate.

though it is more complicated due to the complex chemical ordering within the Heusler alloy. Therefore, we will first treat, in extensive details, the growth of Cr on MgO and use the drawn conclusions when presenting the epitaxial growth of CFA on MgO.

The Cr films were deposited using standard DC magnetron sputtering on polished MgO (001) substrates in a system having a base pressure better than $4x10^{-9}$ torr. The Ar working gas pressure was maintained at 1.0 mtorr during sputtering and the deposition rate was around 0.1nm/s. The substrate temperature during growth was varied between room temperature (RT) and 600 °C.

High angle specular X-Ray diffraction scans were performed to test the orientations present in the different Cr films. figure 2 shows a typical XRD symmetric scan for the Cr film grown at a substrate temperature of 400°C showing only the (002) film reflection. Regardless of the growth temperature, no evidence of other orientation, except for (002) was found. The inset in figure 2 shows the evolution of the Cr (002) peak with the growth temperature. A large decrease of the Cr (002) peak intensity and position shift can be observed for the sample grown at RT relative to the high temperature deposited ones. This suggests the occurrence of an important change in the structure at atomic level for this sample. Figure 3 shows the evolution of the in-plane and out-of-plane lattice parameters as a function of the growth temperatures extracted from symmetric and asymmetric X-Ray diffraction experiments. A 3.2% expansion of the out-of-plane lattice parameter from the bulk value is observed for the sample grown at RT. This growth with the out of-plane lattice expansion is not accompanied by clear in-plane lattice contraction, the small variation of the in-plane lattice parameter from the bulk value being within the measurement error limits. Nevertheless, a small increase of the in-plane lattice parameter can be argued. This behavior is consistent with the in-plane constant expansion due to the tensile strain in the growth plane produced by the lattice mismatch between MgO and Cr (-3.15%).

The out-of-plane lattice distortion is rather difficult to explain. A similar growth temperature dependence of the lattice parameter was observed in triode sputtered V (001) epitaxial films on MgO (001) substrates (Huttel et al., 2005). A complex experimental analysis accompanied with *ab-initio* simulations (Huttel et al., 2007) showed that this low temperature out-of-plane lattice expansion is a metastable state and that it is most likely due to the inhomogeneous disorder created by the bombardment of the growing film by neutral atoms reflected off the target. Another possible mechanism for the lattice expansion is the residual stress of the thin films produced by sputtering at low pressures (Thornton &

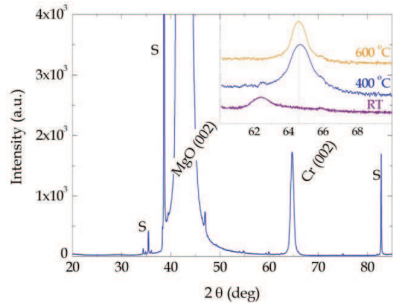

Fig. 2. High angle symmetric scan for the MgO (001)//Cr (16.5nm) film grown at 400°C, showing the presence of Cr (002) reflection, in addition to the MgO (002) one. The peaks marked with S are substrate refections corresponding to the Cu Kα and WLα wavelengths. The inset shows the Cr (002) peak for films deposited at different temperatures. The vertical dashed line marks the position of the Cr bulk 002 reflections. The scans are shifted vertically for better visibility.

Hoffman, 1989). At low sputtering pressures, because of the poor thermalization, there is an increase in high energy atoms arriving at the substrate and, due to the momentum transfer, Cr atoms are forced to into spaces too small to accommodate them under existing thermal equilibrium conditions and, as a result, an out-of-plane lattice expansion takes place (Hsieh et al., 2003). Following these assumptions, one should expect that a substrate temperature increase drives the system to its most stable state relaxing the strains and disorder (Huttel et al., 2007). This is indeed the case and for the sample grown at 400 °C a much smaller strain is observed, the out-of-plane lattice parameter being contracted by 0.12% while the in-plane lattice parameter expanded by 0.18% and, consistent with the in-plane tensile stress to the Cr to MgO lattice mismatch. Moreover, for the sample grown at 600 °C the strain is totally relaxed, most likely by formation of misfit dislocations, and the in-plane and out-of-plane lattice parameters are being consistent with the bulk values.

As expected, the epitaxial quality of the Cr(001) films improves with increasing the growth temperature. The full width at half maximum (FWHM) of the rocking curves around Cr (002) and (011) reflections as a function of temperature are depicted in figure 3b. The figure indicates a FWHM of 0.74° for the (002) reflection and of 0.91° for the (011) reflection, for the sample deposited at 600 °C. These values are in agreement with the previously reported ones (Harp. & Parkin, 1994; Harp. & Parkin, 1996; Fullerton, 1993) and demonstrate a high degree of epitaxy.

The main conclusion from the structural point of view is that it is possible to obtain epitaxial Cr(001) thin films on MgO(001) substrates by DC sputtering starting from room temperature and with improved crystalline quality at higher growth temperatures. Conventionally, it is considered that the epitaxial growth of Cr on insulating substrates by sputtering can be achieved only when the deposition takes place at elevated temperatures (Harp. & Parkin,

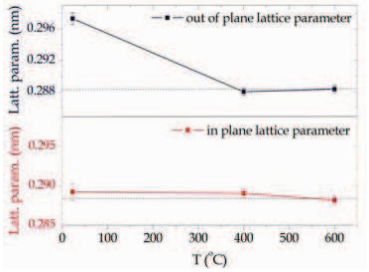

(a)

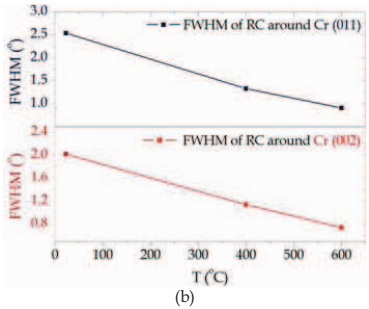

(b)

Fig. 3. (a) Evolution of the in-plane and out-of-plane lattice parameters of the Cr films with the growth temperature and of the (b) full width at half maximum of the rocking curves around Cr symmetric (002) and asymmetric (011) reflections.

1994; Harp. & Parkin, 1996; Fullerton et al., 1993a, 1993b), while our findings show a lower growth temperature required for epitaxy. This behavior is most likely related to our specific growth conditions which imply a relative low Ar pressure during deposition. In contrast to evaporation methods, sputtering deposition methods are characterized by an impulse transfer from accelerated energetic particles to the surface atoms of the target. The energy distribution of the sputtered species has a maximum around 5-10eV, presenting a high energy tail with a low percentage of high energy sputtered particles as well, that can increase by decreasing the Ar pressure (Depla & Mahieu, 2008). It has been shown that these energetic particles can modify the growth kinetics trough the formation of a high density of nucleation centers resulted from their energetic impact on the sample surface (Kalff et al., 1997). The maximum of the sputtered particles energy distribution can be shifted to lower energies by the thermalization process (Meyer et al., 1981), i.e. collisions with the working gas atoms between the target and the substrate. The

thermalization process is controlled by the total gas pressure in the sputtering chamber. Thus, by decreasing the Ar pressure, the thermalization is reduced, so the energy of the atoms arriving at the substrate increases, and eventually, they will have enough energy to undergo diffusion on the surface to a high-binding energy site at a lower surface temperature. The higher mobility of the ad-atoms, together with the increase in the density of nucleation centers, would explain why lower growth temperatures are required for epitaxy to occur under our specific growth conditions.

Atomic force microscopy (AFM) was used to investigate the effect of the deposition temperatures on the films surface morphology. Figure 4 shows the AFM images for Cr films grown on MgO (001) at different temperatures. The deposition of Cr at room temperature yields a very flat featureless surface with a root mean square roughness (RMS) of 0.14 nm. As the temperature is increased to 400 °C and 600 °C, temperature dependent morphological features start to form. The surface of the 400 °C grown sample exhibits 3D rounded islands, while the surface of the 600 °C grown sample display larger, well defined and regulated ones, with the sides parallel to the substrate [110] and to the [1-10] directions. At the same time, the RMS increases from 0.45 nm for the film deposited at 400 °C to 1.25 nm for the film grown at 600 °C.

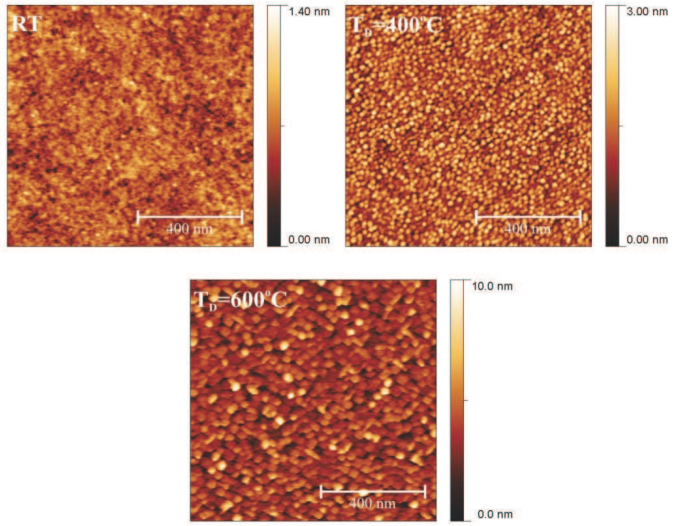

Fig. 4. AFM images (1x1 μm^2 scans) showing the morphology of the MgO(001)//Cr(001) films grown at different temperatures.

It is a common feature for the mid to late transition metals that in conditions of thermodynamic equilibrium not to wet an oxide surface (Campbell, 1997). However, our growth conditions are far from thermodynamic equilibrium and in this case the film growth process is governed by kinetic effects. In a simplified picture layer by layer growth occurs when additional islands start to form on the surface after the previous layer has coalesced. Therefore, in order to prevent nucleation before coalescence, the *ad-atoms* have to be mobile enough to reach the island edges and to have enough energy to overcome the Ehrlich-Schwoebel energetic barrier (Ehrlich & Hudda, 1966; Schwoebel, 1969) encountered by the *ad-atom* upon descending a step. In the special case of non-wetting metals on oxides, the energetics has two essential features: the strong attraction to the edge of an island due to the lateral metal-metal bonding (Ei) and the energy difference (ΔE) between the absorption energy of a metal atom a oxide site and on a metal site (Campbell, 1997; Ernst et al., 1993). If the energy difference (ΔE) exceeds the lateral metal-metal bonding energy (Ei), then there will be no stable sites at the edges of the 2D islands and 3D clusters will form starting from the lowest coverage. On the other hand, if the energy difference (ΔE) is smaller than the lateral metal-metal bonding energy (Ei), the ad-atoms will stick to the edges of the 2D islands, provided that thermal energy is high enough for the ad-atom migration across the surface and for the down-stepping to occur.

Moreover, the up-stepping activation barriers, which is approximately equal to the lateral metal-metal bonding energy (Ei) have to be large as compared to the thermal energy, so that the thermal thickening of the islands to be kinetically disallowed. This pseudo layer-by-layer growth mode usually leads to the formation of 2D islands below a critical coverage, after which additional layers grow in a layer-by-layer mode on top of these islands.

The critical coverage is directly related to the density of 2D islands which is, in turn, linked to the density of nucleation centers. In sputtering deposition, the low percentage of high energy sputtered particles that can reach up to hundreds of eV of energy leads to the formation of a high density of nucleation centers (Kalff, 1997). This will eventually increase the critical coverage giving rise to the formation of at continuous layers at relative low growth temperatures. The arguments above, of kinetically governed growth, can explain the observed morphology of the Cr film deposited at room temperature (see figure 4). As the growth temperature increases, the ad-atoms have enough energy to surface diffuse overcoming the up-stepping energetic barrier, allowing the system to move in the actual thermodynamic equilibrium configuration of 3D islands on the MgO surface (see figure 4). The sample grown at 600 °C exhibits square shaped 3D crystalline clusters with the sides parallel to the substrate [110] and [1-10] directions proving the 45° in-plane rotation epitaxy (see figure1) of Cr on MgO. Another interesting feature of the 3D islands is the narrow size distribution. This aspect is connected with strain and strain relief mechanism. In lattice mismatched epitaxy, after an island is formed, the misfit strain relaxation in the island causes a strain concentration at the edges which increases monotonically with increasing island size. Since the ad-atoms tend to diffuse from the high strain sites to lower strain sites, the strain concentration at the edges will translate into an additional kinetic barrier for the ad-atoms to diffuse to the islands, thus the island growth rate is slowed down as the island size increases, leading to the formation of homogenously sized islands (Chen & Washburn, 1996).

The main result from the X-Ray Diffraction and Atomic Force Microscopy studies is that crystallinity improvements of Cr films deposited on MgO comes with the cost of surface morphology quality (see figures 5, 6 and 7). Since epitaxy is favored at high temperatures, while at surfaces al low temperatures it is difficult to select deposition temperatures that allow for both high degree of epitaxy and flat surfaces. However, the sample deposited at room temperature exhibits very good morphologic properties, while preserving the epitaxy. Therefore, to overcome the challenge of growing Cr films with both flat surface and high degree, one can choose to deposit the films at room temperature and to subsequently perform high temperature annealing stages. Figure 5 shows AFM images for two samples one deposited at room temperature, and the other one deposited at room temperature and post-annealed in vacuum at 600 °C for 20 minutes. As indicated by the images, the post-annealing process preserves and even improves the surface morphology, the root mean square roughness being reduced from 0.17 nm down to 0.12 nm after annealing. As indicated by the X-Ray diffraction measurements (see figure 3), the as deposited film shows a rather large tetragonal lattice distortion that is associated with the growth process. After annealing the film at 600 °C the distortion is relaxed and the in-plane and out-of-plane lattice parameters regain the bulk value. The epitaxial quality of the film increases with annealing, as reflected by the decrease of the FWHM of the rocking-curve around the (002) reflection from 2.54° to 1.51°. The crystallinity also increases after annealing, the mean crystallite size reaching a value comparable with the thickness of the film (16.5 nm). Figure 6 shows a High Resolution Transmission Electron Microscopy (HRTEM) image of a Cr film deposited on MgO at room temperature and subsequently annealed at 600 °C. The image confirms the high quality single crystalline nature of the Cr film.

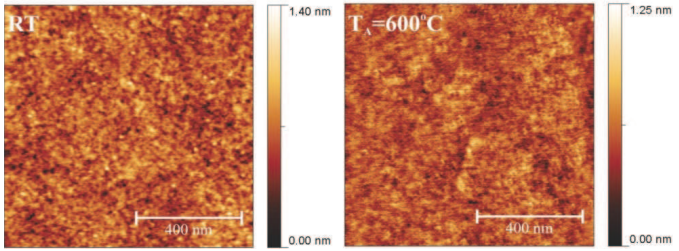

Fig. 5. AFM images (1x1μm^2 scans) showing the morphology of the MgO(001)//Cr(001) films grown at room temperature and post annealed at 600 °C.

In conclusion, we showed that in order to obtain smooth epitaxial Cr films on MgO(001), by sputtering deposition, a two step process must be employed. First, the deposition must take place at low temperatures, to obtain textured films with a flat surface morphology. Secondly, in order to improve the structural properties of the films, a high temperature annealing stage must be performed. Following this procedure, the flat surface morphology is preserved, while the structural properties of the films are improved.

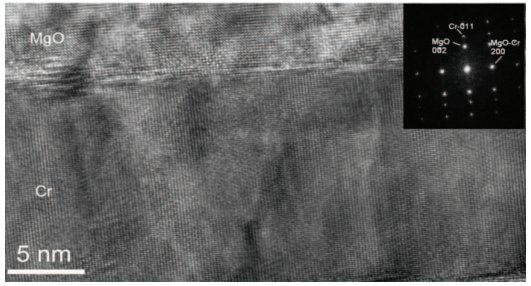

Fig. 6. High Resolution Transmission Electron Microscopy image of an MgO//Cr film deposited at room temperature and annealed at 600°C, confirming the single crystalline growth of Cr on MgO (by courtesy of E. Snoeck CEMES, TOULOUSE).

2.2 Co_2FeAl (CFA) epitaxial films

In a first stage we deposited CFA Heusler alloy thin films on un-buffered MgO(001) single crystal substrates by RF and DC sputtering. As in the case of Cr films, before deposition, the substrates were degassed in-situ at 600°C for 20 minutes. After cooling down to room temperature, a 5 nm thick MgO coating layer was deposited on the substrate. The CFA films with a thickness of 50 nm were sputtered at room temperature from a stoichiometric target ($Co_{50\%}Fe_{25\%}Al_{25\%}$) at 30 W under an Ar pressure of 1 mtorr.

As seen in the case of the Cr buffer layer, depositing the films at high temperatures will increase the crystalline properties but also will degrade the surface morphology through the formation of large 3D clusters. In order to test if this is also valid for CFA we have grown two types of films: one consisting of films deposited at high temperatures and the other of films grown at room temperature and subsequently high temperature vacuum annealed. The surface morphology of the layers was studied by Atomic Force Microscopy and the results are depicted in figure 7.

As seen from the figure 7 the films deposited at high temperatures have a granular structure with increasing grain size for higher deposition temperatures. In the case of the films grown at room temperature and ex-situ post annealed the surface is very flat and featureless, this characteristic being maintained even after annealing at 600 °C. Figure 8 shows the evolution of the Root Mean Square (RMS) surface roughness parameter and of the Maximum Peak-Valley (M_{PV}) distance for CFA films deposited at various substrate temperatures and for CFA films grown at room temperature and ex-situ vacuum annealed. In the case of the annealed samples the RMS and the MPV remain at low values regardless of the annealing temperature. Still, a minimum of RMS of 0.13 nm and M_{PV} of 1.48 nm is obtained for the sample annealed at 400 °C, with a small increase of RMS to 0.18 nm and of the M_{PV} to 2.8 nm for the layer annealed at 600°C. In case of the samples deposited at various substrate temperatures, the RMS and the M_{PV} distance show a monotonous increase from RMS=0.13 nm and M_{PV} =1.48 nm, for the RT deposited sample, to RMS=8.3 nm and M_{PV} =64 nm, for

the films grown at 600°C. For the latter, the M_{PV} distance is even larger than the expected film thickness (50 nm). As seen form figure 7 the film consists of very large 3D clusters and most likely that the layer is not even continuous. This is expected since in conditions of thermodynamical equilibrium the metallic films have the tendency not to wet an oxide surface (see discussion in the previous paragraph).

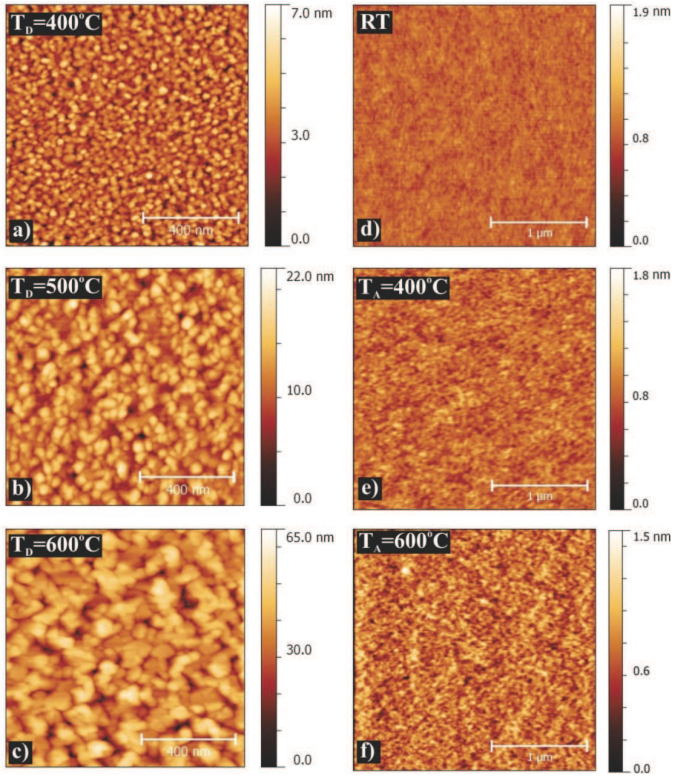

Fig. 7. AFM images showing the surface morphology of CFA films deposited at high temperatures (a), (b) and (c) and deposited at room temperature (d) and ex-situ vacuum annealed (e) and (f).

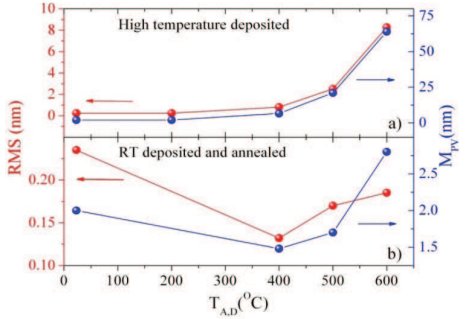

Fig. 8. Evolution of the Root Mean Square (RMS) surface roughness parameter and of the Maximum Peak-Valley (M_{PV}) distance as a function of temperature for (a) CFA films deposited at various substrate temperatures and (b) for CFA films grown at room temperature and ex-situ vacuum annealed.

Our analysis indicated that, due to the granular morphology, the CFA films deposited at high temperatures are not compatible with the manufacturing of magnetic tunnel junctions. Therefore, our efforts have been focused on the room temperature deposited and subsequently annealed samples. The 2θ/ω specular X-Ray diffraction measurements (see figure 9 (a) indicated that the CFA films are epitaxial even when deposited at room temperature and that the crystalline quality of the films increases with annealing (see figure 9 b), the best crystalline properties being obtained for the film annealed at 600 °C. However, the morphological properties of the film annealed at 600 °C are somewhat degraded relative to the one annealed at 400 °C, making the choice of the optimal annealing temperature relative difficult, since both the crystalline and morphological properties of the CFA films are of extreme importance for the further development of the magnetic tunnel junction multilayer stack.

In addition to the films deposited directly on MgO we have grown epitaxial CFA films using a Cr buffer layer. The buffer layer, with a thickness of 20 nm, was deposited as described in the previous section. To ensure a high crystalline quality of the buffer layer, after growth the Cr film was annealed *in-situ* at 600 °C. After cooling down to room temperature the CFA films, with a thickness of 50 nm, were deposited by RF sputtering under 1.0 mtorr of Ar working pressure. As in the case of the films grown directly on MgO, the 2θ/ω specular X-Ray diffraction measurements (see figure 10 a) indicated that the CFA films are epitaxial even when deposited at room temperature and that the crystalline quality of the films increases with annealing (see figure 10 b), the best crystalline properties being obtained for the film annealed at the highest temperature.

An interesting feature is that the values of the FWHM for the samples deposited on the Cr buffer layer are smaller as compared to the ones recorded for the films deposited directly on MgO (figure 9). This is a direct consequence of the smaller lattice misfit between CFA and

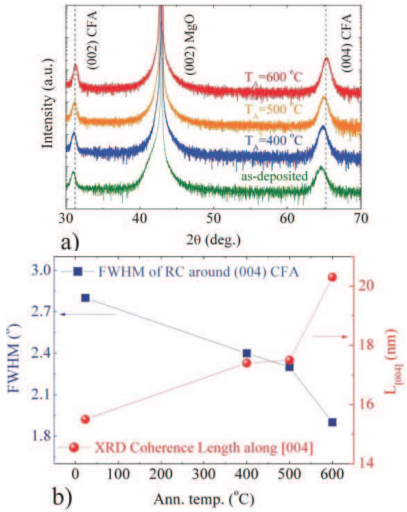

Fig. 9. (a) Specular 2θ/ω X-Ray diffraction patterns for the CFA films as a function of the annealing temperature; (b) FWHM of the rocking curve around the (004) CFA reflection and of the X-Ray diffraction coherence length along [004] direction versus the annealing temperature.

Cr (-0.7%), the one than between CFA and MgO (-3.8%). If the lattice misfit is higher, the interfacial strain energy also increases. This energy is normally relaxed by the formation of dislocations in the film, which, of course, degrade the crystallinity of the epilayer. This is also sustained by the evolution of the mean size of the X-Ray coherently diffracting domains as a function of annealing temperature. The mean size has the same behavior, as in the case of MgO deposited CFA films (figure 9), correlating perfectly with the decrease of the FWHM, but the values are larger for the Cr buffered films. The increased size of the coherently diffracting domains indicates that the epitaxial perfection of the CFA lattice is spread over larger distances, the density of lattice dislocations being lower than in the case of the films grown on MgO.

The surface morphology of the CFA films deposited by RF sputtering on Cr buffered MgO substrates was investigated by Atomic Force Microscopy. Figure 11 shows AFM images for the CFA films as-deposited at room temperature and post-annealed at 600 °C for 20 minutes. One can see that the surface of both films are very flat and featureless. For the as deposited film, the RMS roughness parameter is around 0.1 nm and slightly smaller for the annealed one. The M_{PV} distance decreases from 1.7 nm, for the as-deposited film, to just less than 1 nm for the

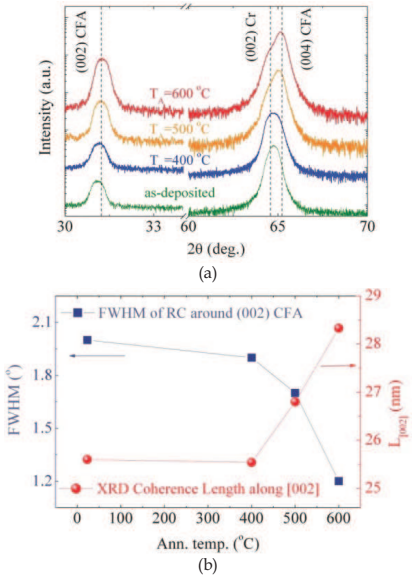

Fig. 10. (a) Specular 2θ/ω X-Ray diffraction patterns for the Cr/CFA films as a function of the annealing temperature; (b) FWHM of the rocking curve around the (002) CFA reflection and of the X-Ray diffraction coherence length along [002] direction versus the annealing temperature, indicating the improvement of the crystallinity of the films with annealing.

annealed one. These results indicate that, contrary to the case of the CFA films deposited directly on the MgO substrate, both the crystalline properties and the surface morphology of the Cr buffered CFA film improve with the increase of the annealing temperature.

The growth of a high quality tunnel barrier in a magnetic tunnel junction is in general a very difficult task since the tunnel barrier must be very thin, typically 1-2 nm, and pinhole free in order to avoid metallic shorts in the junction. This implies that the lower electrode of the junction to be extremely flat, which is indeed the case of the Cr buffered CFA film annealed at 600°C. Using this optimized lower electrode we have grown the subsequent MgO tunnel barrier and the upper CoFe electrode. The AFM measurements have indicated a very flat morphology for the tunnel barrier (see figure 12 a), with a RMS roughness around 0.2 nm, which ensure the continuity of the barrier, as also suggested by the HRTEM images in figure 12 b. Moreover, the HRTEM images indicate that the whole magnetic tunnel junction stack is epitaxial.

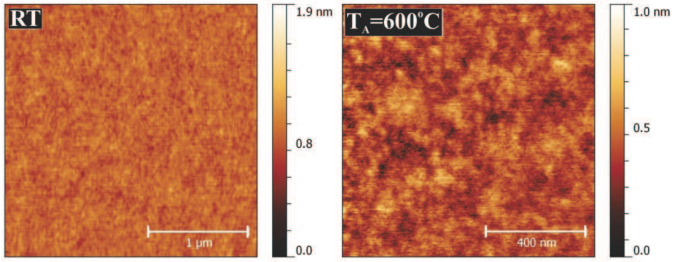

Fig. 11. AFM images of Cr buffered CFA films as-deposited at room temperature and post-annealed at 600°C for 20 minutes.

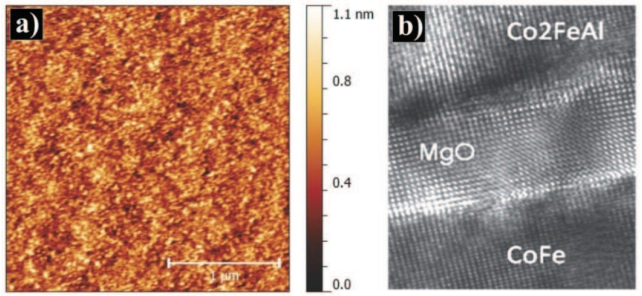

Fig. 12. (a) AFM image on the MgO//Cr(15 nm)/CFA(20 nm)/MgO(2.2 nm) stack indicating the morphology in the tunnel barrier; b) High Resolution Transmission Electron Microscopy image of the magnetic tunnel junction indicating the crystallinity and continuity of the barrier.

Based on this analysis, we succeeded to grow and pattern by optical lithography magnetic tunnel junctions which give significant tunnel magnetorezistive effects at room temperature.

3. The use of AFM/MFM techniques for the study of hybrid interface systems between high temperature superconductors and magnetic structures

Concerning the second part of the chapter, we present the magnetic force microscopy as a powerful tool to get deep insight in the micro-magnetic properties of a magnetic thin film interfaced with a high temperature superconductor layer. More recently, a new hybrid research domain has emerged: superconducting spintronics, dealing with systems constituted by alternating superconducting and magnetic layers. The aim of these novel

systems is to drive new functionality of the constituent layers by taking profit on the mutual interfacial interaction between the superconductor and the magnetic film. For instance, vortices and the anisotropy of the electronic transport in the superconductor can be controlled by the stray-fields emerging from a modulated magnetic structure (Carneiro 2007, Hoffman et al 2008, Karapetrof et al 2009). The engineering of the micromagnetic properties in continuous or patterned magnetic thin films represent therefore a powerful tool to control the electronic transport in the superconductor. We illustrate the results concerning the modulation of the magnetic structure of Permalloy thin films via the thickness of the film. We follow the evolution of the magnetization from in-plane to out-of-plane by increasing the thickness and we present a direct correlation between the micromagnetic properties, measured by MFM, and the magnetic properties at macroscopic scale (magnetization hysteresis curves) measured by standard magnetometry. Furthermore, we exemplify the possibility to engineer the magnetic/micromagnetic properties in mezoscopic size magnetic objects patterned by optical lithography. Single objects and arrays of circular shape of mezoscopic dots with lateral size in the micron range, are considered. Alternatively, nanoscopic magnetic objects are elaborated using polystyrene balls shadowing/lift-off technique.

In the past decade numerous research groups have addressed the problem of magnetic pinning in superconductors (Aladyshkin et al., 2009). The relevance of this subject lies in the possibility of attaining large pinning forces of vortices in type II superconductors, that are temperature independent, through the interaction between the vortex flux and the magnetization of a magnetic structure, *i.e.* ferromagnetic films, ferromagnetic micro-, or nanostructures.

Large scale applications of superconductivity, such as energy transport, superconducting magnets, engines, generators, etc., require superconducting materials with a critical current density, J_c, greater than 1 MA/cm² and high irreversibility lines. In order to fulfill these requirements, the only way is to avoid the vortex motion, which is responsible for the energy dissipation in a type II superconductor. Up to date, the method used to block the vortex movement is their pinning on normal impurities present in a superconductor, the so-called *normal core pinning*. This type of pinning relies on the tendency of the vortex normal core to attach itself to regions in the superconductor where superconductivity is suppressed, in an attempt to minimize the overall system energy. For this reason, normal zones within the superconductor are artificially created in different ways. These zones coexist with the natural occurring normal regions arising from inherent growth defects, such as grain boundaries, dislocations and the presence of secondary phases. Several ways of externally inducing normal regions in superconductors have been demonstrated. They include: irradiation by swift heavy ions, artificially introduced regular arrays of holes, artificially introduced nanoparticles that create columnar defects in superconducting films, or surface decoration of the substrate upon which the superconducting film is grown (Civale et al., 1991; Augieri et al., 2010; Mele et al.,2006; Sparing et al., 2007). However, classic non-magnetic pinning becomes ineffective at high temperatures making it difficult to imagine practical applications of HTS materials.

In this context, magnetic pinning, originating from the Zeeman interaction between a magnetization and the magnetic flux of the SC vortices, may be a valid alternative for

effective vortex pinning applications, as the pinning potential created by a magnetic structure, in this case displaying a stripe domain structure varying along the x axis, is expressed as

$$U_{mp} = \Phi_0 M(x) d_s \tag{3}$$

d_s being the superconducting layer thickness and $M(x)$ the magnetization value, which, neglecting the domain wall contributions, takes the values of $\pm M_0$ (Bulaevskii et al., 2000). Even though the above expression of the pinning potential is calculated for a particular case of magnetic configuration, the point it stands for may be generalized to any magnetic distribution, and it is that magnetic pinning potential is independent of temperature. Of course, the Curie temperature of the ferromagnet has to be high enough so that there is no significant variation of the magnetization with temperature, in the superconducting regime of the SC film. This fact makes this type of pinning as the ideal case of superconducting vortex pinning, suitable for high temperature superconductors. Equating the magnetic pinning force, calculated from the pinning potential (3), as U_{mp}/l, with l as the domain width, to the Lorentz force acting on the vortex line, stemming from the transport current in the SC layer, $J\Phi_0 d_s/c$, gives a rough estimate of the critical current

$$J_c \sim cM_0 / l. \tag{4}$$

It can be seen that within the model proposed, the critical current density, J_c, increases as the perpendicular component of the magnetization, M_0 increases, justifying the use in magnetic pinning experiments FM structures that exhibit a perpendicular anisotropy.

In the following paragraphs we give an account of the results obtained on some magnetic systems exhibiting out-of-plane anisotropy investigated for possible magnetic pinning applications of superconducting vortices. They include permalloy continuous thin films, permalloy micronic disks and cobalt nanostructures. A particular emphasis is placed on the magnetic characterization of the above structures by means of magnetic force microscopy (MFM) and the information this analysis may give regarding the magnetic pinning characteristics of the respective investigated systems.

3.1 Permalloy thin films

In the case of Permalloy, Py, ($Ni_xFe_{(1-x)}$, x=19-21 at.%) thin films, perpendicular anisotropy originates from a negative magnetostriction constant correlated with an in- plane tensile strain of the films. In this case, the anisotropy constant is given by the expression (Saito et al., 1964):

$$K_U = \frac{3}{2}\lambda_L \sigma \tag{5}$$

where λ is the magnetostriction constant and σ represents the strain of the film.

The orientation of the magnetization within Py thin films is determined by the competition between the perpendicular anisotropy energy term and the magnetostatic energy. Since the uniaxial anisotropy is not strong enough to determine the perpendicular orientation of the magnetization with respect to the film surface, the resulting configuration corresponds to an out-of-plane deviation of the magnetization. The domain pattern stabilized by this

orientation is comprised of stripes in which the magnetization points alternatively, outwards and inwards with respect to the film surface, Figure 13. Because the deviation angle, θ, of the magnetization is less than 90º, this domain configuration is referred to as a *weak stripe* domain pattern. A consequence of the presence of weak stripe domains is the so called *rotatable anisotropy*. This phenomenon consists in the orientation of the domain stripes along the direction of a relatively weak, in-plane applied magnetic field, and the persistence of this orientation after the field is removed. The field magnitude is typically of few hundreds of Oe. The two properties of thin Py films recommend them for fundamental studies of magnetic pinning in superconductors, as they allow for the preparation of two different states with respect to the effects of vortex pinning, as illustrated in Figure 14. These two states consist in the parallel and perpendicular orientation of a current density, ***J***, which is injected into a superconducting $YBa_2Cu_3O_7$ (YBCO) strip, with respect to the orientation of the magnetic stripe domains of a Py film deposited on top. As it can be seen, the Lorentz-type force acting on the superconducting vortices is directed perpendicularly to the current density. For the perpendicular configuration, Figure 14a, the vortices will not be acted upon by any pinning force as the vortex motion takes place along the stripe domains where the magnetization is constant. This configuration is referred to as a *vortex guide* configuration. On the other hand, in the parallel configuration, Figure 14b, the force due to the current density acts on the vortices so as to move them across the magnetic domains. In this case the vortex motion will be impeded by the presence of the periodic modulation of the magnetization. Thus, the vortices will by pinned by a periodic magnetic pinning potential. In order to be able to fabricate and study such systems, a careful analysis of the magnetism of the Py thin films is required. For this purpose we have fabricated several polycrystalline thin Py films by means of dc magnetron sputtering, deposited on Si (111) single crystal substrates. The thickness of the films was varied between 270 and 720 nm. The as deposited films were analyzed by means of vibrating sample magnetometry (VSM) and magnetic force microscopy (MFM).

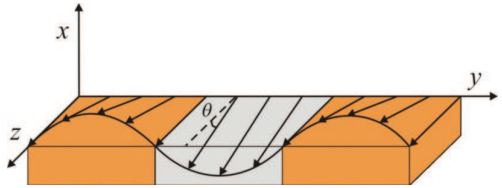

Fig. 13. Schematic representation of the spin distribution within the weak stripe domain configuration, as proposed by Chikazumi (Chikazumi, 1997). It is to be noted that the out-of-plane component of the magnetization has a sine variation along the y direction. The out-of-plane deflection angle of the spins is denoted by θ.

The magnetization dependence on the externally applied field, Figure 15, has the characteristic shape of the films that exhibit weak stripe domains. The magnetic field was applied parallel to the film surface plane. The linear decrease of the magnetization from saturation is observed with a small hysteresis. The decrease is due to the out-of-plane rotation of the film magnetization, corresponding to the weak stripe formation. The

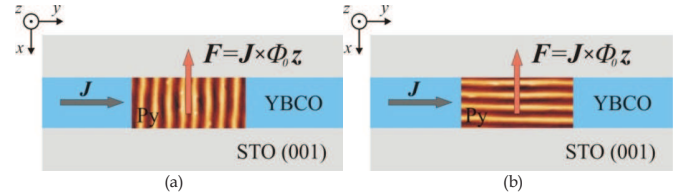

Fig. 14. Schematic representation of the vortex guide (a) and the periodic pinning potential (b) configurations of a Py/YBCO heterostructure.

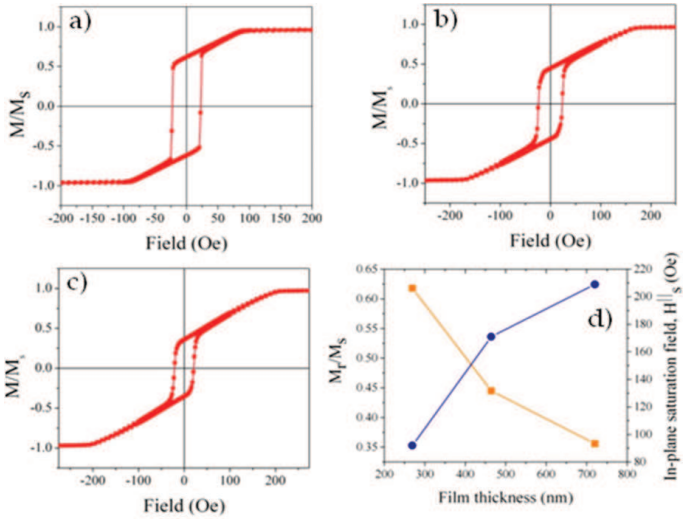

Fig. 15. Hysteresis loops of the (a) 270 nm, (b) 646 nm and (c) 730 nm thick Py thin films. The shape of the loop is typical for films having weak stripe domain configuration; (d) Variation of the normalized remanent magnetization, M_r/M_s, and of the in-plane saturation field, $H||_{sat}$, as a function of Py film thickness.

hysteresis on the other hand, may be explained by the existence of a slight difference in the stripe domain pattern in the two branches.

In order to test the expected rotatable magnetic anisotropy, the cycles were performed applying the magnetic field in two different perpendicular directions. No modification of

the loops were observed, proving thus the existence of rotatable anisotropy. Figure 15d presents the thickness dependence of two characteristic magnetic quantities, the magnetization at remanence, M_r, and the in-plane saturation field, $H^{||}_{sat}$. As the film thickness increases, the magnetostatic energy of surface charges decreases, allowing for the perpendicular anisotropy to manifest by an increase of the deviation angle of the spins, θ, with respect to the film surface plane. This increased deviation leads to a decrease of the in-plane magnetization remanence. Consequently, the larger magnetization perpendicular to the film plane leads to a higher in-plane saturation field. With respect to our goal to fabricate and study hybrid interface SC/FM systems for vortex pinning, higher θ values are expected to have a more pronounced influence on the superconducting properties of the bottom SC layer. Concomitantly, as analytical calculations have shown (Saito et al., 1964, Chikazumi, 1997, Murayama, 1966), an increase of film thickness also leads to an increase of stripe periodicity, *i.e.* domain width. In the following we present the results of MFM measurements on the film domain structure and how it is affected by the film thickness.

The domain structure of the films having thicknesses of 270 nm, 460 nm and 720 nm are shown in Figure 16. As it can be seen, the expected stripe domain configuration is present. Extracting a profile from the above images allows for an evaluation of the stripe wavelength, λ, and accordingly, of the domain width, $d=\lambda/2$, Figure 17. The domain width variation as a function of thickness has also been calculated according to the three models (Saito et al., 1964, Chikazumi, 1997, Murayama, 1966). For the calculation, the physical parameters entering the domain width expression were taken from (Ben Yousseff et al., 2004), so that M_s=826 emu/cm^3, the out-of-plane anisotropy constant, K_U=5×10^4 erg/cm^2, while the exchange stiffness constant was taken to be A=1×10^{-6} erg/cm. Comparing the measured results with the three models, it is noted that the initial model of stripe domains, proposed by Saito et al. (Saito et al., 1964), in which the spin direction varies perpendicularly to the stripes in a *zig-zag* as a function of position, is the worst approximation to the domain width value. A sine variation (Chikazumi, 1997) of the spin direction yields a better approximation of the domain width. Yet, the best results are found using the model proposed (Murayama, 1966). Because of the fact that their model allows for the highest freedom in spin ordering, allowing for a variation of the spins with respect to all the coordinate axes, they are able to take into account the presence of closure domains at film surface. As confirmed by numerical simulations run on low out-of-plane anisotropy Py thin films (Vlasko-Vlasov et al., 2008, Ben Yousseff et al., 2004), the model proposed by Murayama is the closest in describing the actual physical picture in these systems, and thus yields the most satisfactory result in predicting the domain width dependence on the film thickness.

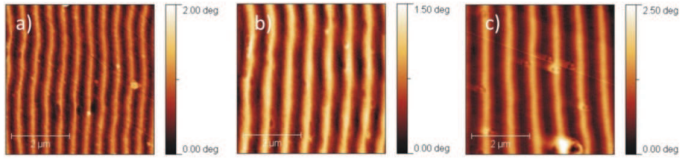

Fig. 16. 5 μm×5 μm MFM images of the (a) 270 nm, (b) 460 nm and (c) 720 nm thick Py films.

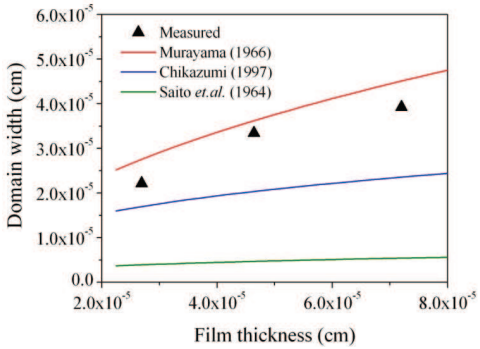

Fig. 17. Domain width of the 270 nm, 460 nm and 720 nm thick Permalloy films. Domain width variation as a function of film thickess, calculated according to the three different models presented in the text.

As far as the rotatable magnetic anisotropy is concerned, Figure 18 shows the orientation of the domain stripes in a remanent state after the application of an in-plane magnetic field along different directions. The value of the applied field was set at 650 Oe in order to ensure saturation of all the studied films. As it can be observed, the stripe domains align themselves along the direction of the applied magnetic field and do not change their orientation after the field is removed. The rotatable anisotropy feature of low out-of-plane anisotropy magnetic thin films is essential for the study of the influence of a periodic magnetic field on the superconducting properties of SC thin films, as it allows for a systematic modulation of the stray magnetic field produced by the FM layer (Belkin et al., 2008).

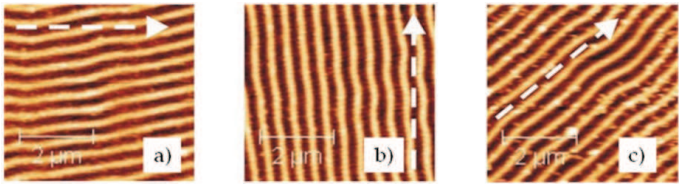

Fig. 18. Rotatable anisotropy. Different magnetic stripe orientations correspond to the direction of the applied magnetic field for a 460 nm thick Py film.

3.2 Magnetic micro,- and nanostructures

Periodic stripes of alternating "up" and "down" orientation of magnetization with respect to the film surface plane are expected to provide a strong pinning of the SC vortices when

these alternations are oriented perpendicularly to the direction of the vortex motion. Magnetic micro,- and nanostructures, such as regular dot arrays, provide an additional degree of freedom to the modulation, as they are also subject to a topographic periodicity, given by the specific pattern of the arrays defined by lithographic techniques. In these sense, even the sole presence of such structures in the vicinity of SC films may give rise to a pinning potential of the vortices, as demonstrated by Hoffmann et al. (Hoffmann et al., 2000) in their study of a Nb film deposited on top of a regular array of non-magnetic Ag dots. The flexibility in defining different configurations of dot lattices coupled with their respective magnetic configurations produce *commensurability effects*.

These effects consist in resonant changes of the magnetoresistance of the SC layer, $\rho(H_{ext})$, with the appearance of equidistant minima having a period in H determined by lattice constant of the magnetic dot arrays. Also, these minima are visible in the field dependence critical current density, $J_c(H_{ext})$, or in the magnetization curves, $M(H_{ext})$. These effects are explained considering a strong magnetic pinning potential exerted by magnetic dots on the SC vortices, coupled with a structural match between the dot and vortex lattices. Thus, when the condition that an integer number of vortices per magnetic unit cell is fulfilled, a maximum number of vortices are pinned, producing resistivity minima or J_c maxima of the SC film. The field dependence of these effects is explained by the fact that the vortex lattice parameter is field-dependent. Because of the fact that the vortex lattice is triangular strong commensurability effects are produced by triangular dot lattice. Lateral structuring of the magnetic films into micro or nanostrucutres also influences their magnetic configuration, so that the magnetic state of the film will be altered when it is patterned into dot sutructures. Jubert and Allenspach (Jubert and Allenspach, 2004) constructed a phase diagram of the magnetic states of circular nanometric dots as a function of their thickness and diameter, based on micromagnetic simulations. By varying the lateral size and thickness of the dots one is able to stabilize different magnetic states: in-plane single domain (IPSD), vortex (V) and out-of-plane single domain (OPSD). Carneiro (Carneiro, 2004) calculated the interaction energy between a SC vortex and an in-plane and out-of-plane magnetized dipole showing that different attraction interaction profiles exist between the dipole and the vortices in the two cases. While in the case of out-of-plane magnetic dipoles the largest pinning potential arises at the center of the dipole, in the case of an in-plane dipole configuration pinning is present at the edges of the object where the variation of the magnetization is highest. Larger, micronic, dots that may be able to accommodate a multi-domain magnetic configuration are also interesting in the study of FM/SC structures as their net magnetic moment may be tuned by magnetizing the sample in a field lower than the saturation field (Aladyshkin et al., 2009). Also larger dots may be able to stabilize "giant" vortices that are able to carry more than one flux quanta (Aladyshkin et al., 2009).

In view of the above arguments, it can be seen that within the context of FM/SC heterostructures, magnetic micro,- and nanostructures present a special importance as they can produce effective magnetic pinning that can be modulated both by the dot lattice, as well as their magnetic state. In this sense we have fabricated micronic Py disks having diameters of 10, 5 and 1μm. Also, Co nanostructures were grown using an alternative lithographic process that involves the use of self-assembled polystyrene nano-spheres as a shadow mask.

3.2.1 Permalloy microstructures

Figure 19 presents the magnetic images of circular, 350 nm thick Py dots having a diameter of (a)10, (b)5 and (c)1 μm. For the 10 μm dots, the diameter is well above the stripe domain width, estimated to be around 300 nm, according to the model proposed by Murayama (Murayama, 1966). As a consequence, the disks exhibit a well defined striped domain pattern. The stripes that are situated at the center of the disk have the same orientation and are very much similar to the case of a continuous film. As the stripes are situated closer to the edge of the microstrucutres, they tend to curve along the side of the dots, so as to prevent any magnetic charge build-up at the edges, and so to reduce the magnetostatic energy of the system. These *closure domain* - type structures have a limited spatial extension with respect to the overall area of the dots. As the diameter of the dots is reduced to 5 μm, even though this dimension is still considerably higher than the domain width, the stripe pattern is almost entirely pertaining to the closure domains. As a consequence, the MFM images of the 5 μm dots is composed of alternating bright and dark concentric circles. Again, locally the parallel stripe order is maintained. However, this is not the only domain configuration that can be observed. Another domain pattern that is observed, resembles the one present in the 10 μm structures. It consists of straight magnetic stripes in the center and elongated circles at the edges as closure domains. It can be noted that the surface "covered" by the closure domains is much larger than in the 10 μm case, reaching 100% for the circular stripe pattern. In view of the evolution that was observed so far, the domain pattern for 1 μm dots is not surprising. As the diameter of the microstructures is reduced towards the limiting value of the stripe width, the competition between the anisotropy and magnetostatic energies results in the formation of stripe domains in the form of concentric rings. For the 1μm disks, the single bright/dark alternation in the MFM images indicates the existence of solely two magnetic domains.

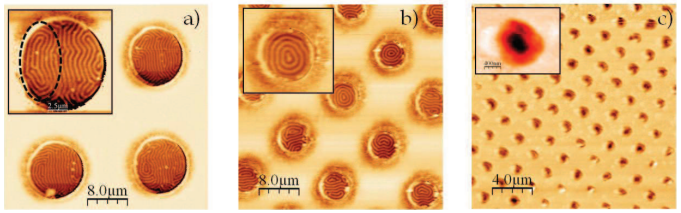

Fig. 19. MFM images of (a)10 μm (40 μm×40 μm), (b) 5 μm (40 μm×40 μm), (c) 1 μm (20 μm×20 μm), Py dots.

3.2.2 Cobalt nanostructures

Co nanostructures were obtained using the polystyrene nanosphere lithography, a method described in detail in (Canpean et al., 2009). 170 nm and 40 nm thick films were deposited on a nanoshpere patterned Si substrate. After lift-off, triangular Co structures remain on the substrate. Even though a large difference in the deposited film thickness was prepared, the height of the nano-structures in the case of the two films did not differ significantly. In the

case of the 40 nm thick film, the mean height of the magnetic structures was of 12 nm, while for the thicker 170 nm film, the resulting dots were only 25 nm high. The large difference in the expected value of the height of the dots and the actual one is probably due to the shadowing effect produced by a divergent beam of sputtered atoms and also by the large diameter of the spheres (450 nm), which accentuate these effects. The MFM analyses performed on the two films are shown in Figure 20. For the 25 nm high structures, the dots are in a mono-domain state. The MFM contrsast consists of a dark/bright formation corresponding to an in-plane magnetic dipole structure. If the initial film thickness is decreased, the magnetic configuration of the nanostructures changes, as can be seen in Figure 20b, into a vortex-like spin configuration. The MFM contrast is typical for nanostructures in this configuration, having a bright center and the rest of the dot exhibiting a darker shade. According to the diameter-thickness phase diagram (Jubert and Allenspach, 2004) both dots should have been in the magnetic vortex state, and moreover the behavior predicted by the phase diagram is that for thicker dots the vortex state becomes more stable for a larger range of dot diameters. Our findings point out a different behavior, in the sense that thicker structures are found to be in the single domain state. Although no concrete explanation was found for this trend, we suspect that the particular shape of the dots, in our case triangular, may play an important role in modifying the magnetic phase diagram.

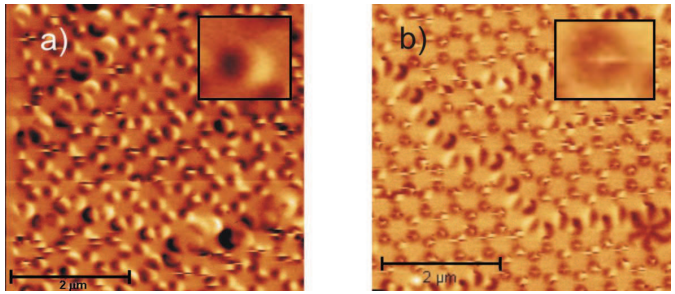

Fig. 20. MFM images of Co nanostructures having different thicknesses: (a) 20 nm (magnetic dipoles) and (b) 12 nm (magnetic vortices).

4. Conclusions

Within this chapter we illustrated the use of the Atomic Force Microscopy techniques as a powerful tool in characterization of complex thin film systems. Usually, when elaborating multilayer thin film stacks, the constituent layers have to be continuous and to present small roughness. Therefore, the AFM characterization will provide important information about the film surface topology in studies related to roughness reduction. Furthermore, high resolution analysis of the film topology can be used in studies of thin film growth mechanisms when the growth parameters (substrate temperature, deposition rate, etc…) are varied. Within the field of the Spintronics, for the elaboration of devices such as the magnetic tunnel junction, the extreme control of roughness of the constituent layers and the

continuity of the insulating tunnel barrier is required. The interfacial roughness induces here fluctuations in electronic transport properties (perpendicular to the stack) with detrimental effects on the functional properties of the MTJ device.

Moreover, the Magnetic Force Microscopy operating mode represents a versatile tool for the characterization of the micromagnetic properties of continuous magnetic thin films or mezoscopic size patterned magnetic objects. We have chosen here to illustrate the use of the MFM for characterizing the micromagnetic features of continuous magnetic films and patterned magnetic objects which started recently to be used for magnetic pinning of superconducting vortices in high temperature superconductors.

5. Acknowledgments

This work has been partially supported by CNCSIS-UEFISCSU, project number PNII IDEI No. 4/2010, code ID-106 and by POS CCE ID. 574, code SMIS-CSNR 12467.

6. References

Aladyshkin, A. Yu; Silhanek, A. V.; Gillijns, W. & Moshchalkov, V. V. (2009). Nucleation of superconductivity and vortex matter in superconductor–ferromagnet hybrids, *Superconductor Sciemce and Technology*, Vol.22, No.5, (May 2009), pp. 053001-053049, ISSN 1361-6668 (online)

Augieri, A.; Celentano, G.; Galluzzi, V.; Mancini, A.; Rufoloni, A.; Vannozzi, A.; Angrisani Armenio, A.; Petrisor, T.; Ciontea, L.; Rubanov, S.; Silva E. & Pompeo, N. (2010). Pinning analyses on epitaxial $YBa_2Cu_3O_7{-}\delta$ films with $BaZrO_3$ inclusions, *Journal of Applied Physics*, Vol.108, Issue 6, (September 2010), pp. 063906-063911, ISSN 1089-7550 (online)

Bulaevskii, L. N.; Chudnovsky, E. M. & Maley, P. M. (2000). Magnetic pinning in superconductor-ferromagnet multilayers, *Applied Physics Letters*, Vol.76, Issue 18, (March 2000), pp. 2594-2597, ISSN 1077-3118 (online)

Ben Youssef, J.; Vukadinovic, N.; Billet, D. & Labrune, M. (2004). Thickness-dependent magnetic excitations in Permalloy films with nonuniform magnetization, *Physical Review B*, Vol.69, Issue 17, (May 2004), pp. 174402-174411, ISSN 1550-235x (online)

Belkin, A.; Novosad, V.; Iavarone, M.; Pearson, J. & Karapetrov, G. (2008). Superconductor/ferromagnet bilayers: Influence of magnetic domain structure on vortex dynamics, *Physical Review B*, Vol.77, Issue 8, (May 2008), pp. 180506(R)-180510(R), ISSN 1550-235x (online)

Canpean, V.; Astilean, S.; Petrisor Jr., T.; Gabor, M. & Ciascai, I. (2009). Convective assembly of two-dimensional nanosphere lithographic masks, *Materials Letters*, Vol.63, Issue 21, (August 2009), pp. 1834-1836, ISSN 0167-577X

Carneiro, G. (2007). Tunable pinning of a superconducting vortex by a magnetic vortex, *Physical Review B*, Vol.75, Issue 9, (March 2007), pp. 094504-094514, ISSN 1550-235x (online)

Campbell, C. (1997). Ultrathin metal films and particles on oxide surfaces: structural, electronic and chemisorptive properties, *Surface Science Reports*, Vol.27, Issues 1-3, (May 1998), pp. 1-111, ISSN 0167-5729

Chen, Y. & Washburn, J. (1996). Structural Transition in Large-Lattice-Mismatch Heteroepitaxy, *Physics Review Letters*, Vol.77, Issue 19, (November 1996), pp. 4046-4049, ISSN 1079-7114 (online)

Chikazumi, S. (1997). *Physics of Ferromagnetism*, Oxford Science Publications, ISBN 0-19-851776-9, New York, United States

Civale, L.; Marwick, A. D.; Worthington, T. K.; Kirk, M. A.; Thompson, J. R.; Krusin-Elbaum, L.; Sun, Y.; Clem, J. R.; Holtzberg, F. (1991). Vortex confinement by columnar defects in $YBa_2Cu_3O_7$ crystals: Enhanced pinning at high fields and temperatures, *Phys. Rev. Lett.*, Vol. 67, Issue 5, (July 1991), pp. 648-651, ISSN 1079-7114 (online)

Depla, D. & Mahieu, S., eds., Reactive Sputter Deposition, Springer Series in Materials Science (2008);

Ehrlich, G. & Hudda, F. G. (1966). Atomic View of Surface Self-Diffusion: Tungsten on Tungsten, *Journal of Chemical Physics*, Vol.44, Issue 3, (February 1966), pp. 1039-1049, ISSN 1089-7690 (online)

Elbaum, L.; Sun, Y.; Clem,J. R. & Holtzberg, F. (1991). Vortex confinement by columnar defects in YBa2Cu3O7 crystals: Enhanced pinning at high fields and temperatures, *Physical Review Letters*, Vol.67, Issue 5, (July 1991), pp. 648-651, ISSN 1079-7114 (online)

Ernst, K. H. ; Ludviksson, A.; Zhang, R.; Yoshihara, J. & Campbell, C. T. (1993). Growth model for metal films on oxide surfaces: Cu on ZnO(0001)-O, *Physical Review B*, Vol.47, Issue 20, (May 1993), pp. 13782-13796, ISSN 1550-235x (online)

Fullerton, E.; Conover, M.; Mattson, J.; Sowers, C. & Bader, S. (1993). Oscillatory interlayer coupling and giant magnetoresistance in epitaxial Fe/Cr(211) and (100) superlattices, *Physical Review B*, Vol.48, Issue 21, (December 1993), pp. 15755-15763, ISSN 1550-235x (online)

Fullerton, E.; Conover, M. J.; Mattson, J.; Sowers, C. & Bader, S. (1993). 150% magnetoresistance in sputtered Fe/Cr(100) superlattices, *Applied Physics Letters*, Vol.63, Issue 12, (July 1993), pp. 1699-1702, ISSN 1077-3118 (online)

Huttel, Y.; Navarro, E. & Cebollada, A. (2005). Epitaxy and lattice distortion of V in MgO/V/MgO(001) heterostructures, *Jounal of Crystal Growth*, Vol.273, Issue 3-4, (November 2004), pp. 474-480, ISSN 0022-0248

Huttel, Y.; Cerda, Y.; Martinez, J. & Cebollada, A. (2007). Role of volume versus defects in the electrical resistivity of lattice-distorted V(001) ultrathin films, *Physical Review B*, Vol.76, Issue 19, (November 2007), pp. 195451-195458, ISSN 1550-235x (online)

Hoffmann, A.; Prieto P. & Schuller, I. K. (2000). Periodic vortex pinning with magnetic and nonmagnetic dots: The influence of size, *Physical Review B*, Vol.61, Issue 10, (March 2000), pp. 6958-6965, ISSN 1550-235x (online)

Hsieh, J.; Li, C.; Wu, W. & Hochman, R. (2003). Effects of energetic particle bombardment on residual stress, microstrain and grain size of plasma-assisted PVD Cr thin films, *Thin Solid Films*, Vol.424, Issue 1, (January 2003), pp. 103-106, ISSN 0040-6090

Harp, G. & Parkin, S. (1994). Seeded epitaxy of metals by sputter deposition, *Applied Physics Letters*, Vol.65, Issue 24, (October 1994), pp. 3063-3066, ISSN 1077-3118 (online)

Harp, G. & Parkin, S. (1996). Epitaxial growth of metals by sputter deposition, *Thin Solid Films*, Vol.288, Issue 1-2, (February 1996), pp. 315-324, ISSN 0040-6090

Jubert, P.-O. & Allenspach, R. (2004). Analytical approach to the single-domain-to-vortex transition in small magnetic disks, *Physical Review B*, Vol.70, Issue 14, (October 2004), pp. 144402-144407, ISSN 1550-235x (online)

Karapetrov, G.; Belkin A.; Novosad V.; Iavarone M.; Pearson J. E. & Kwok W. K. (2009). Adjustable superconducting anisotropy in MoGe-Permalloy hybrids, *Journal of Physics: Conference Series*, Vol.150, Part 5, pp. 052095-052099, ISSN 1742-6596 (online)

Kalff, M.; Breeman, M.; Morgenstern, M.; Michely, T. & Comsa G. (1997). Effect of energetic particles on island formation in sputter deposition of Pt on Pt(111), *Applied Physics Letters*, Vol.70, Issue 2, (January 1997), pp. 182-184, ISSN 1077-3118 (online)

Murayama, Y. (1966). Micromagnetics on Stripe Domain Films. I. Critical Cases, *Journal of the Physical Society of Japan*, Vol. 21, pp. 2253-2266, ISSN 1347-4073 (online)

Mele, P.; Matsumoto, K.; Horide, T.; Miura, O.; Ichinos, A.; Mukaida, M.; Yoshida Y. & Horii, S. (2006). Tuning of the critical current in $YBa_2Cu_3O_{7-x}$ thin films by controlling the size and density of Y2O3 nanoislands on annealed SrTiO3 substrates, *Superconductor Science and Technology*, Vol.19, No.1, (November 2006), pp. 44-50, ISSN 1361-6668 (online)

Meyer, K.; Schuller, I. & Falco, C. (1981). Thermalization of sputtered atoms, *Journal of Applied Physics*, Vol.52, Issue 9, (September 1981), pp. 5803-5805, ISSN 1089-7550 (online)

Saito, N. ; Fujiwara, H. & Sugita, Y. (1964). A New Type of Magnetic Domain in Thin Ni-Fe Films, *Journal of the Physical Society of Japan*, Vol.19, pp. 421-422, ISSN 1347-4073 (online)

Sparing, M.; Backen, E.; Freudenberg, T.; Hühne, R.; Rellinghaus, B.; Schultz L. & Holzapfel, B. (2007). Artificial pinning centres in YBCO thin films induced by substrate decoration with gas-phase-prepared Y2O3 nanoparticles, *Superconductor Science and Technology*, Vol. 20, No.9, (September 2007), pp. S239-S246, ISSN 1361-6668 (online)

Schwoebel, R. L. (1969). Step Motion on Crystal Surfaces. II, *Journal of Applied Physics*, Vol.40, Issue 2, (February 1969), pp. 614-618, ISSN 1089-7550 (online)

Tiusan, C.; Greullet F.; Hehn M.; Montaigne F.; Andrieu S. & Schuhl A. (2007). Spin tunnelling phenomena in single-crystal magnetic tunnel junction systems, *Journal of Physics: Condensed Matter*, Vol.19, No.16, (April 2007), pp. 165201-165235, ISSN 1361-648X (online)

Thornton, J. & Hoffman, D. (1989). Stress-related effects in thin films, *Thin Solid Films*, Vol.171, Issue 1, (April 1989), pp. 5-31, ISSN 0040-6090

Vlasko-Vlasov, V.; Welp, U.; Karapetrov, G.; Novosad, V.; Rosenmann, D.; Iavarone, M.; Belkin, A. & Kwok, W.-K. (2008). Guiding superconducting vortices with magnetic domain walls, *Physical Review B*, Vol.77, Issue 13, (April 2008), pp. 134518-134524, ISSN 1550-235x (online)